Precise temporal control of a GEVI's conformation enables the visualization of charge migration in a fluorescent protein resulting in an improved optical response

Lee Min Leong[1], Jun Kyu Rhee[1], Heejung Kim[1,2], Jihye Seong[1], Junhyuk Woo[1], Kyungreem Han[1], Douglas Storace[3], and Bradley J. Baker[1,4]

1. Brain Science Institute, Korea Institute of Science and Technology, Seoul, Republic of Korea

2. Department of Converging Science and Technology, Kyung Hee University, Seoul, Republic of Korea

3. Department of Biological Science, Florida State University, Tallahassee, Florida

4. Division of Bio-Medical Science and Technology, KIST School, Korea University of Science and Technology (UST), Seoul, South Korea

Abstract

Electrodynamic pathways through the fluorescent protein domain enable the genetically encoded voltage indicator (GEVI) ArcLight and its derivatives to optically report conformational changes induced by membrane potential transients. These electrical pathways through the fluorescent protein domain of Super Ecliptic pHluorin exhibit remarkable precision as demonstrated by the divergent optical behavior of Gln versus Asn mutations. At position D147 on the external surface of the fluorescent protein domain, Gln exhibits a voltage-dependent behavior like other negatively charged acidic amino acids at that location while the Asn mutant exhibits a response similar to the charged positive amino acids at that position. Replacement of Thr with Gln at the 203 position with the amino acid side chain in close proximity to the internal chromophore does not affect the speed of the voltage-dependent optical signal, but replacement with Asn slows the voltage-dependent optical signal implicating a twisting of the chromophore in response to transient charge interactions on the exterior of the β-can being altered during the voltage-induced conformational change. In addition to polar amino acids affecting these electrodynamic pathways, hydrophobic residues play a noticeable role in the migration of charge from the exterior of the fluorescent protein to the chromophore potentially by shielding/creating inducible dipoles on the surface of the fluorescent protein. Using these novel insights, a new GEVI that gets significantly brighter upon depolarization of the plasma membrane was developed enabling voltage imaging of population signals with low light levels at a frame rate of 5 kHz in acute brain slice as well as the reporting of neuronal activity *in vivo*.

Introduction

The molecular interactions of amino acids with its environment, be it an aqueous solution, a lipid membrane, and/or other amino acids ultimately determine the structure and function of a protein. The combination of these interactions ranging from van der Waal forces to hydrogen bonds and ionic salt bridges fold the protein into a functioning unit capable of staggering diversity from ion transport to

immunological surveillance to enzymatic catalysis to name a scant few. These interactions create a stable framework to maintain biological integrity (i.e., substrate affinity) while also enabling flexibility to accommodate conformational changes required for function (i.e., catalysis).

Structural determination of proteins has provided insights into how these molecular interactions enable protein function. Highly resolved structures are capable of identifying potential hydrogen bonds allowing models to predict the biophysical consequences of these electrostatic interactions. Fluorescent proteins (FPs) are ideal for such modeling as the fluorescent properties of the protein are influenced by the electrostatic environment surrounding the chromophore. For example, the long Stokes shift observed in avGFP is the result of a proton wire that shuttles a proton from the protonated chromophore [1-4]. Upon excitation at 390 nm, the protonated chromophore rapidly undergoes an excited state proton transfer at the picosecond timescale that deprotonates the chromophore resulting in emission at 505 nm. While protein structure is critical for identifying potential electrostatic interactions and understanding how a protein functions, it provides only a snapshot of a stable conformation. Of further interest would be the rapid and reversible alteration of the electrostatic environment throughout a protein in order to study how the protein responds.

The fluorescent biosensor ArcLight [5] is a genetically encoded voltage indicator (GEVI) that optically reports conformational changes induced by transient alterations in the plasma membrane potential. Depolarization of the plasma membrane decreases ArcLight's fluorescence while hyperpolarization causes ArcLight to become brighter. The ArcLight protein (Figure 1A) consists of a voltage-sensing domain (VSD) from the *Ciona intestinalis* voltage-sensing phosphatase attached to the pH-sensitive FP, Super Ecliptic pHluorin (SEpH) [6]. SEpH is dim under acidic conditions and bright at neutral and alkaline pH. However, the pH sensitivity of SEpH is not sufficient for generating ArcLight's large, voltage-dependent optical signal (see insert in Figure 1A) [5]. A mutation on the external surface of the β-barrel of SEpH, A227D (numbering of amino acids throughout is based on the position in the GFP protein), is also required. While the role of this negative charge on the surface of the FP is unclear, the mutations rendering SEpH pH sensitive involve side chains oriented on the outer surface of the β-barrel as well. Pathways must therefore exist that convey external charge conditions on the outer surface of the β-barrel structure to the internal chromophore creating an optical dependence on pH or, in the case of ArcLight and the A227D mutation, membrane potential.

Several lines of evidence suggest that the pathway(s) conveying charge information through the FP domain of ArcLight are altered when the VSD responds to membrane potential transients. Repositioning the negative charge originally located at A227D along the exterior of the β-barrel inverted the polarity of the voltage-dependent optical signal [7]. The position of the external negative charge determined whether the GEVI got dimmer or brighter upon depolarization of the plasma membrane. The VSD in the plasma membrane has also been shown to dimerize [8] enabling intermolecular Förster Resonance Energy Transfer (FRET) between ArcLight-derived GEVIs having a FRET donor FP or a FRET acceptor FP when co-expressed in the cell (Figure 1B) [9]. Dimerization of ArcLight via the VSD could bring neighboring FP domains in close proximity allowing the negative charge on the surface of the SEpH A227D mutant to commandeer the pH response of a nearby chromophore. Voltage-induced

conformational changes would then alter the position of the negative charge relative to a neighboring chromophore thereby affecting its fluorescence.

The possibility that the optical response of ArcLight involves changes to the electrostatic environment of the chromophore was recently demonstrated by mutations to a proton wire involving the chromophore of SEpH A227D. An ArcLight-derived GEVI with the additional E222H mutation to the FP domain exhibited a voltage-dependent increase in the 505 nm emission wavelength when excited at 390 nm [7]. Since the protonated chromophore excited at 390 nm requires a proton wire for deprotonation of the chromophore and subsequent emission at 505 nm, the voltage-dependent increase in emission upon 390 nm excitation revealed a temporal modulation of the internal electrostatic environment around the chromophore mediated by voltage-induced conformational changes of the GEVI.

In order to facilitate the temporal modulation of the electrostatic environment near the chromophore, we have sought to investigate potential pathway(s) charge migrates across the exterior of the β-barrel to the internal chromophore. ArcLight-derived GEVIs are ideal for this purpose as multiple conformational changes can be induced with millisecond temporal precision via whole cell patch clamp. Exploring these interactions, we have found that a combination of hydrophilic and hydrophobic amino acids on the surface of the β-barrel is capable of altering the voltage-dependent optical signal. In addition, modulation of the internal electrostatic environment does not necessarily alter the protonation state of the chromophore. Instead, the chromophore likely twists resulting in GEVIs that get dimmer or brighter depending on the initial planarity and subsequent twisting of the chromophore.

Exploiting this mechanism, we have created a novel GEVI with a large voltage-dependent signal, Ulla that gets brighter upon depolarization of the plasma membrane. Optical signals from Ulla were detected in brain slice experiments using low LED illumination at a recording frame rate of 5 kilohertz. In addition, highly reproducible single trial evoked *in vivo* signals from the mouse olfactory bulb have been observed. Ulla should therefore be a useful tool for monitoring voltage transients in neuronal circuits and sets the stage for manipulating the electrodynamic pathways of other FPs.

A

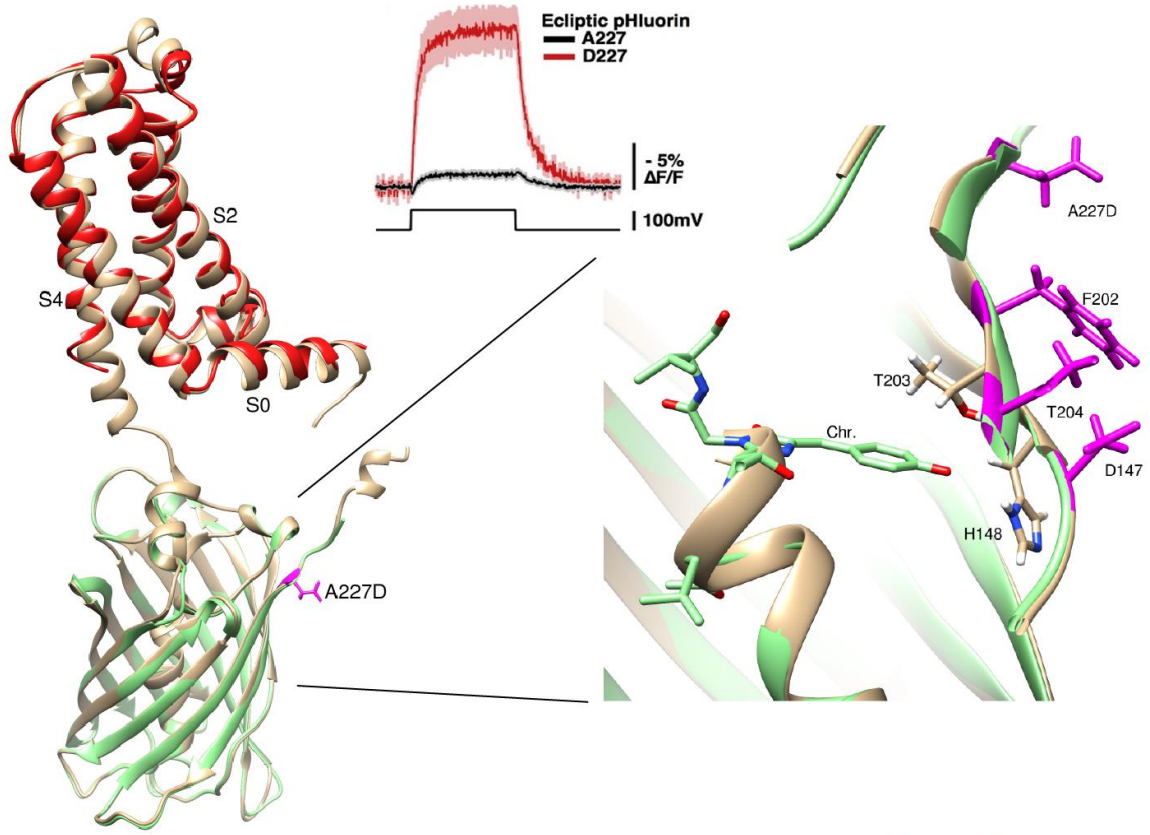

B

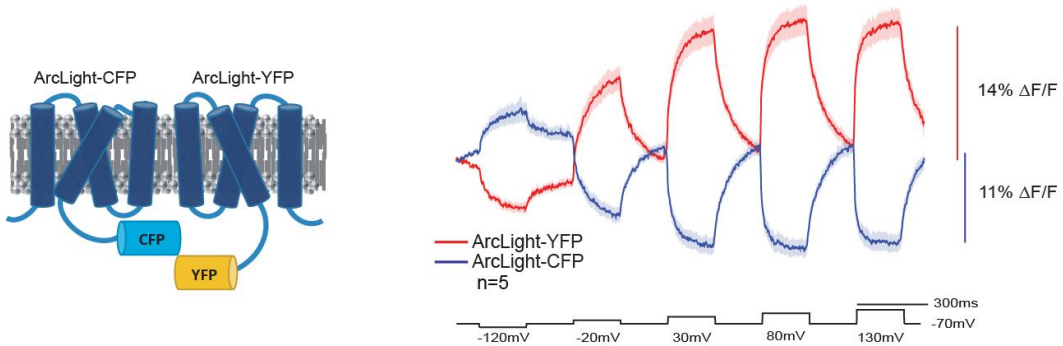

Figure 1. A. Alphafold prediction of ArcLight and the effect of the A227D mutation on the voltage-dependent optical signal. The ArcLight prediction (beige) from Alphafold [10] is overlaid with the crystal structure of the VSD from the voltage-sensing phosphatase (red, PDB 4g7v [11]) and the crystal structure of GFP (green, PDB 4eul [12]). The VSD resides in the plasma membrane consisting of four transmembrane segments (S1-S4). S0 is an α-helix that resides in the cytoplasm near the plasma membrane. The random coil N-terminus of the predicted ArcLight structure from Alphafold has been removed for clarity. The FP domain of ArcLight resides in the cytoplasm and is fused to the VSD by a

linker region. The optical traces reproduced with permission from Jin et al., 2012 [5] illustrate the large improvement in the voltage-dependent optical signal for the A227D mutation in SEpH for ArcLight. The A227D mutation is shown in magenta. Zoomed structure on the right highlights the exterior position of A227D in SEpH as well as three other amino acids (also in magenta) known to be important for the large voltage-dependent optical signal of ArcLight [13]. Note that while the Alphafold prediction shows a high degree of overlap with both the VSD and GFP crystal structures, it does not perform the autocatalytic reaction that generates the chromophore. Therefore, only the chromophore from the GFP crystal structure is shown for reference. **B. Intermolecular FRET of ArcLight variants.** When the FP in ArcLight is changed to CFP and co-transfected with an ArcLight-YFP version, altering the membrane potential affects the FRET efficiency suggesting that the A227D mutation in the FP domain of the original ArcLight is interacting with a neighboring FP domain. Reproduced with permission from Leong et al., 2021 [9].

Materials and Methods

Plasmid design and construction. The Triple Mutant and Bongwoori GEVIs are as described in Piao et al., 2015 [14]. The ArcLight construct is as described in Jin et al., 2012 [5], and the BongwooriR3 construct is as described in Lee et al., 2017[15]. Primers were designed to introduce the point mutations to the FP as required. Conventional one-step and two-step PCR were used to generate the target inserts. The inserts were cloned into the vector using NEB restriction enzymes. The backbone vector used in this study is pcDNA3.1 (Invitrogen) with a CMV promoter.

Cell culture and transfection. HEK 293 cells were cultured in Dulbecco's Modified Eagle Medium (DMEM; Gibco, USA) supplemented with 10% Fetal Bovine Serum (FBS; Gibco, USA) in a 37 °C, 100% humidity and 5% CO_2. For transfection, HEK 293 cells were suspended using 0.25% Trypsin-EDTA (Gibco, USA) then plated onto poly-L-lysine (Sigma-Aldrich, USA) coated #0 coverslips (0.08-0.13mm thick and 10 mm diameter; Ted Pella, USA) at 70% confluency. Transient transfection was carried out with Lipofectamine 2000 (Invitrogen, USA) according to the manufacturer's protocol.

Viral injection and slice preparation. Virus injection and slice preparation were done according to an approved animal experiment protocol by the Institutional Animal Care and Use Committee at KIST (animal protocol 2019-099). 4-week-old C57BL/6N male mice were anesthetized by 1.5%-3% isoflurane. Adeno-associated virus (AAV) AAV2/1-hSyn-Ulla was then injected into the CA1 region of the hippocampus bilaterally as described previously (Lowery & Majewska, 2010). Recordings were performed at least 2 weeks after the injection.

300 mm thick acute coronal brain slices were prepared following the NMDG protective recovery method (Ting et al., 2018). Halothane (Sigma, USA) was used to anesthetize the mice before euthanasia. The isolated mouse brain was sliced in ice-cold high-sucrose artificial cerebrospinal fluid (ACSF) solution (75 mM Sucrose, 25 mM $NaHCO_3$, 2.5 mM KCl, 0.5 mM $CaCl_2$, 7 mM $MgCl_2$, 1.25 mM NaH_2PO_4, 87 mM NaCl and 25 mM D-glucose) gassed with 95% O_2/5% CO_2 to give a pH of 7.4 using the VT-1200

Vibratome (Leica, Germany). Slices were then allowed to recover for at least an hour in a chamber filled with ACSF, incubated at 36 °C.

Electrophysiology. Coverslips with transiently transfected cells were inserted into a patch chamber (Warner instruments, USA) sealed with a #0 thickness cover glass for simultaneous voltage clamp and fluorescence imaging. The chamber was kept at 34 °C throughout the experiment and perfused with bath solution (150 mM NaCl, 4 mM KCl, 1 mM MgCl2, 2 mM CaCl2, 5 mM D-glucose and 5 mM HEPES, pH = 7.4). Filamented glass capillary tubes (1.5mm/0.84mm; World Precision Instruments, USA) were pulled by a micropipette puller (Sutter, USA) prior to each experiment to pipette resistances of 3–5 MΩ for HEK 293 cells and 3–6 MΩ for cultured primary neurons. The pipettes were filled with intracellular solution (120mM K-aspartate, 4 mM NaCl, 4 mM MgCl2, 1 mM CaCl2, 10 mM EGTA, 3 mM Na2ATP and 5 mM HEPES, pH = 7.2) and held by a pipette holder (HEKA, Germany) mounted on a micromanipulator (Scientifica, UK). Whole cell voltage clamp and current clamp recordings of transfected cells were conducted using a patch clamp amplifier (HEKA, Germany). A holding potential of −70 mV was used for all recordings including neuronal recording with cultured neurons until switched to current clamp mode.

Fluorescence microscopy of cultured cells. An inverted microscope (IX71; Olympus, Japan) equipped with a 60X oil-immersion lens with 1.35-numerical aperture (NA) was used for epifluorescence imaging. The light source was a 75 W Xenon arc lamp (Osram, Germany) placed in a lamp housing (Cairn, UK). GFP was imaged using a filter cube consisting of an excitation filter (FF02-472/30-25), a dichroic mirror (FF495-Di03) and an emission filter (FF01-496) for the 470 nm wavelength excitation. All filters and dichroic mirrors are from Semrock (USA). Two cameras were mounted on the microscope through a dual port camera adapter (Olympus, Japan). A slow speed color charge-coupled-device (CCD) camera (Hitachi, Japan) was used to visualize cells during patch clamp experiments. Fluorescence changes of the voltage indicators were typically recorded at 1 kHz frame rate by a high-speed CCD camera (RedShirtImaging, USA) unless otherwise specified. All the relevant optical devices were placed on a vibration isolation platform (Kinetic systems, USA) to avoid any vibrational noise during patch clamp fluorometry experiments.

Data acquisition and analysis. Resulting images from patch clamp fluorometry were acquired and analyzed for initial parameters such as fluorescence change [ΔF = Fx−F0] or fractional fluorescence change values (ΔF/F = ((Fx−F0)/F0) * 100) by NeuroPlex (RedShirtImaging, USA) and Microsoft Excel (Microsoft, USA). The acquired data from whole cell voltage clamp experiments of HEK 293 cells were averaged for 16 trials (technical replication) unless otherwise noted. The number of recorded cells in this work is biological replicates and the number of trials averaged for each HEK 293 cell should be interpreted as technical replication. Data were collected from recorded cells that did not lose their seals during the whole cell voltage clamp recording. ΔF/F values for the tested voltage pulses were plotted in OriginPro 2016 (OriginLab, USA). A ΔF/F trace versus time graph for each cell was also fitted for either double or single exponential decay functions in OriginPro 2016 as described previously (Piao et al., 2015).

Slice imaging in dorsal hippocampal CA1 region

Coronal slices of BL6 mouse brain injected with AAV2/1-hSyn-Ulla 2 weeks prior to the experiment were prepared following the NMDG protective recovery method, and the dorsal hippocampal CA1 region of the BL6 mouse expressing hSyn-Ulla was imaged during a Schaffer collateral stimulation using bipolar electrodes (FHC, Bowdoin, ME). Brain slice recording were carried out 33 °C with the recording chamber continuously perfused with ACSF. The stimulus timing trigger and recording were done using Multiclamp 700B amplifier (Molecular devices, USA).

Each hSyn-Ulla recording was either acquired at 1 kHz as 80 pixel x 80 pixel or at 5 kHz as 26 pixel x 26 pixel fluorescence intensity time-lapse images using an upright epifluorescence microscope (Slicescope, Scientifica, East Sussex, UK) equipped with a High-speed CCD camera (Neuro CCD, RedShirtImaging, Decatur, GA), a GFP filter set (GFP-3035D-OMF, Semrock, Rochester, NY), a 10x water immersion objective lens (UMPlanFL N; NA=0.3, Olympus, Tokyo, Japan), and a 1.3 mW/cm^2 460 nm LED light source (UHP-Mic-LED-460, Prizmatix, Givat-Shmuel, Israel). The fluorescence intensity trace of hSyn-Ulla was low pass filtered using a 50 Hz 5th order Butterworth filter, baseline prior to stimulation fitted with an exponential decay curve and normalized to %ΔF/F fractional fluorescence. A single recording or 5, 10, or 20 recordings were averaged to derive the average hSyn-Ulla response curve. The frame subtracted hSyn-Ulla intensity images were pseudocolored by manually setting the colored intensity range from +0.3 %ΔF/F to -0.2 %ΔF/F and spatially low pass filtering with a 3 pixel x3 pixel mean filter.

In vivo imaging.

Surgical procedures. All experimental procedures were approved by the FSU ACUC. C5/BL6 mice (3 female, 1 male, 4 months old) were anesthetized with ketamine/xylazine (90/10mg/kg), and given dexamethasone and atropine, and lacrilube was applied to their eyes. Anesthetic depth was monitored during all surgical procedures via pedal reflex. The body temperature of the animals was maintained at 37.5 by placing a heating pad underneath the animal. For virus injections, an incision was made in the skin above the olfactory bulb, and a small craniotomy was made. 500nl of AAV-syn-ulla was injected into the olfactory bulb over a period of 15 minutes. Mice were given the analgesic rimadyl for 3 days following surgery. For imaging procedures, a head-post was attached to the top of the skull using metabond (Parkell, Edgewood, NY). The skull above the dorsal olfactory bulbs was either thinned and covered with cyanoacrylate to improve optical clarity, or removed and replaced with a glass coverslip.

Imaging. Imaging was carried out using a custom epifluorescence microscope built from Thorlabs (Newton, NJ) components with a 35mm or 50mm CCTV lens. Illumination was provided by a Prizmatix LED (UHP-T-LED-455) filtered with a 488/10 nm (Semrock FF01-488/10). A dichroic mirror (59009bs, Chroma) directed the excitation light towards the preparation, and transmitted the fluorescence emission through a band-pass filter (Chroma 59009m), before being recorded using a DaVinci 1k camera (RedShirtImaging, Decatur, GA). Imaging was carried out between 40-200 Hz at a spatial resolution of 256x256 pixels.

Olfactometer. A flow-dilution olfactometer was placed in front of the animal's nose. The odor methyl valerate (acquired from Sigma-Aldrich) was diluted using a custom flow-dilution olfactometer at concentrations between 1-6 % of saturated vapor.

Histology. Mice were euthanized with euthasol, and their brains were dissected and left in 4% paraformaldehyde for a minimum of 3 days. The brains were embedded in agarose and cut on a vibratome in 50 µm coronal sections before being mounted. Slides were examined on a Zeiss Axioskop (Carl Zeiss Microsystems).

Data analysis.

Odorant-evoked signals were collected in consecutive trials separated by a minimum of 60 seconds. Ulla signals representing depolarization are shown as upward signals. Data from each pixel were low-pass Gaussian filtered at 2 Hz and had an exponential drift subtracted that was calculated based on the signal prior to the stimulus onset (exponential subtraction function in NeuroPlex). The signal from each pixel was divided by its resting fluorescence measured at the beginning of each trial. The fluorescence brightness analysis was measured by choosing a region of interest that captured the entire surface of the injected and uninjected hemibulbs. The mean fluorescence in the initial 2 seconds of the imaging trial was measured in both hemibulbs in 4 trials and averaged together. The results were normalized to the fluorescence in the uninjected hemibulb and averaged across all four preparations. The ΔF/F analysis was carried out by subtracting a 1-s window around the peak of the odor response from the 2-s immediately preceding the odor stimulus. This measurement was carried out in 4-5 trials per preparation before being averaged together.

Results

Four amino acids in the FP domain of ArcLight have been implicated in the voltage-dependent optical response [13] (Figure 1A). Introducing a combination of SEpH mutations into EGFP (S147D/S202F/Q204T) as well as the ArcLight specific A227D mutation were sufficient and necessary for achieving a large voltage-dependent optical signal when fused to the VSD of ArcLight [13]. While all four amino acids have side chains external to the β-can structure, the three mutations found in SEpH (S147D, S202F, and Q204T) flank amino acids with internal side chains near the chromophore, H148 and T203 (Figure 1A). Since the A227D mutation is necessary for the large voltage-dependent signal but not required for the pH sensitivity and is far removed from the chromophore, we postulated that D147, F202, and Q204 in SEpH were somehow involved in transmitting external charge conditions to the internal chromophore.

Side chain composition at position 147 in the FP domain influences the voltage-dependent optical signal.

When the SEpH mutation, S147D, was introduced into EGFP, the pKa was altered [13]. To explore the possibility that the A227D mutation in ArcLight was commandeering the pH response of a neighboring FP domain, we mutated D147 of SEpH in the ArcLight-derived GEVI, TM [14]. TM is a faster version of ArcLight with a longer linker segment of amino acids between the VSD and the FP domain. Distinct patterns in the voltage-dependent optical response depending upon the side chain chemistry of the amino acid introduced at the 147 position were seen when these mutants were expressed in HEK 293 cells and subjected to whole cell voltage clamp (Figure 2A). The D147T, D147S, and D147Q mutants yielded voltage responses very similar to the original D147 version. The maximal change in fluorescence

was 9% $\Delta F/F$ for the D147S mutant and 8% $\Delta F/F$ for the D147Q mutant with both exhibiting slightly slowed optical responses. The weighted τ_{on} was 18.2 ± 1.1 msec for D147S while the weighted τ_{on} was 13.1 ± 0.8 msec for D147Q. In contrast, the D147K and the D147N constructs yielded a much reduced change in fluorescence consisting of at least two components. The initial decline in fluorescence in response to a depolarization step of the plasma membrane was followed by a slow increase in fluorescence. Upon a return to the holding potential, the fluorescence overshot the original baseline and slowly descended back.

While the voltage-dependent optical signal of the D147Q mutant was very similar to the original D147, the optical activity of the D147N mutant exhibited a voltage-dependent pattern like that for the positively charged amino acids at 147. Gln and Asn have the same functional carboxamide side chain group with the side chain differing in length by a single alkyl group. The orientation of the carboxamide determined the voltage-dependent optical pattern observed when the plasma membrane was depolarized. The oxygen moiety of the sidechain was involved for the D147Q mutant (as well as the D147, D147S, D147T mutants) while the nitrogen moiety affected the D147N and the D147K mutants voltage-dependent optical behavior.

With the ability to functionally resolve the orientation of the side chain chemistry at D147, we resorted to Alphafold [10] to glean potential insights into the role the amino acid side chain at position 147 plays since there is no crystal structure for SEpH. Interestingly, mutating D147 also affected the position of the H148 side chain in the interior of the β-barrel structure for the Alphafold predictions while having no noticeable effect on the positioning of the Q149 side chain (Figure 2A). The predicted structures for the D147X mutants are overlaid with the original D147 version of SEpH to show the variability/flexibility of the H148 position. The Alphafold predictions for D147K and D147N show a rotation of H148 when compared to the original D147 structure prediction in relation to the internal chromophore. The D147T, D147S, and D147Q predictions all show a very similar position for H148 which is oriented much like the original D147.

While the position of H148 apparently correlated to the pattern of the voltage-dependent optical signal, the situation is more complex as revealed by the behavior of aromatic amino acids at the 147 position (Figure 2B). The D147Y mutant showed a completely different voltage-dependent signal than the other polar amino acids tried at that position. Upon depolarization of the plasma membrane, the optical signal of the D147Y mutant actually increased. The change in fluorescence was small, but the optical signal had clearly inverted. Signal inversion was also observed upon the introduction of other aromatic amino acids at position 147. When the non-aromatic, non-polar alanine was substituted into position 147, the signal for D147A looked very similar to the original D147 version despite the rotated orientation of H148 (Figure 2B).

A role for hydrophobic amino acids in determining electrodynamic pathways in proteins.

With the aromatic residues at position 147 exhibiting a unique voltage-dependent optical response, we sought to further investigate the role hydrophobicity may play in affecting the voltage-dependent

optical signal. F202 (Figure 1A) is one of the required residues identified for the large optical signal of ArcLight in response to voltage [13]. In EGFP, the polar amino acid, Ser, resides at position 202 suggesting that for a pH-dependent fluorescence response of SEpH a combination of polar and non-polar residues are important for directing charge from the surface of the FP to the internal chromophore. We therefore introduced non-polar, non-aromatic amino acids into the F202 position. Lowering the degree of hydrophobicity/reducing the surface area of the side chain at position 202 had a dramatic effect on the voltage-dependent optical signal (Figure 3). The F202L and F202V mutants had substantially reduced voltage-dependent signals while the F202I mutant once again reversed the polarity of the signal albeit very weakly.

A.

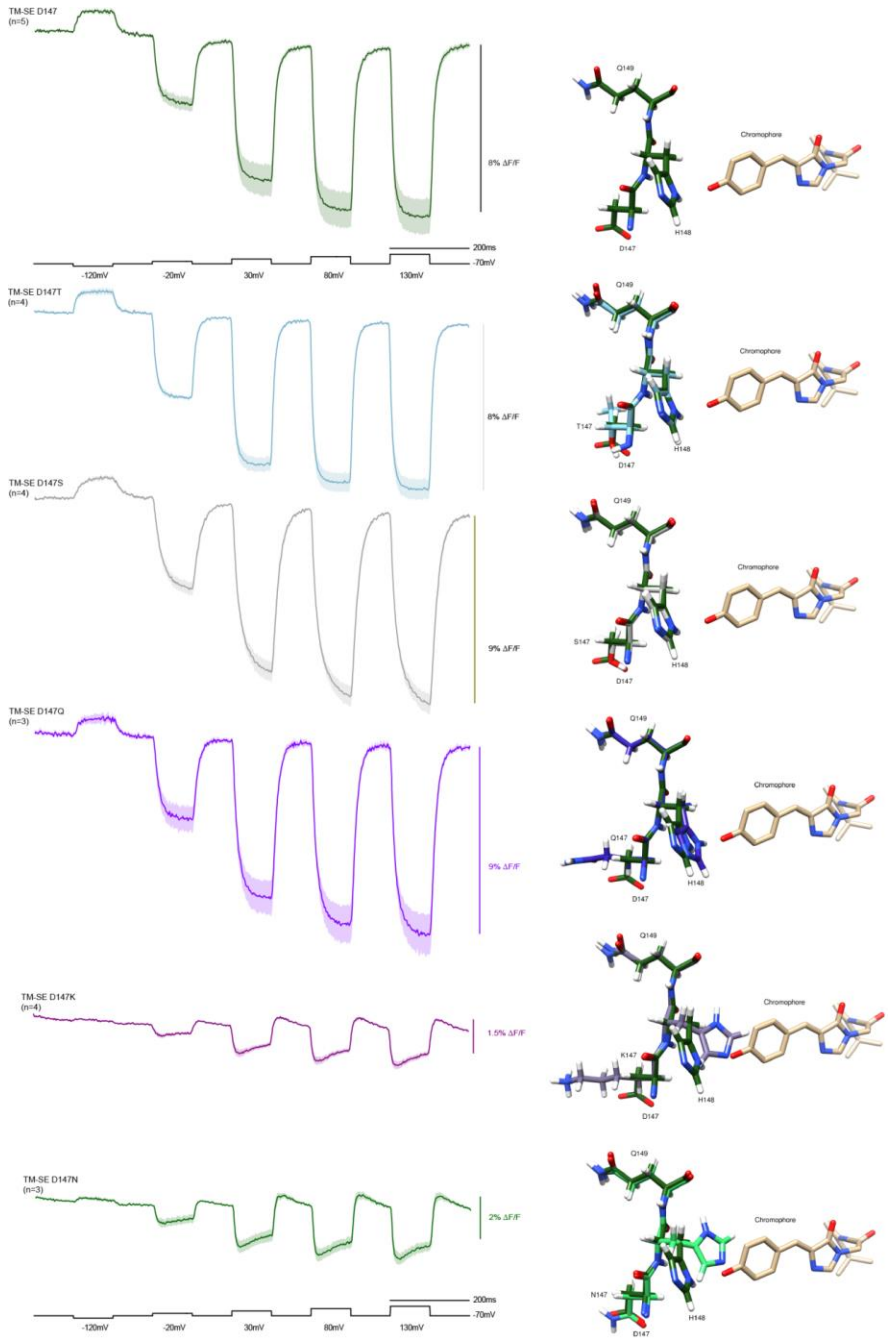
TM-SE D147
(n=5)
8% ΔF/F
200ms
-70mV
-120mV
-20mV
30mV
80mV
130mV
Q149
Chromophore
D147
H148
TM-SE D147T
(n=4)
8% ΔF/F
T147
TM-SE D147S
(n=4)
9% ΔF/F
S147
TM-SE D147Q
(n=3)
9% ΔF/F
Q147
TM-SE D147K
(n=4)
1.5% ΔF/F
K147
TM-SE D147N
(n=3)
2% ΔF/F
N147

B.

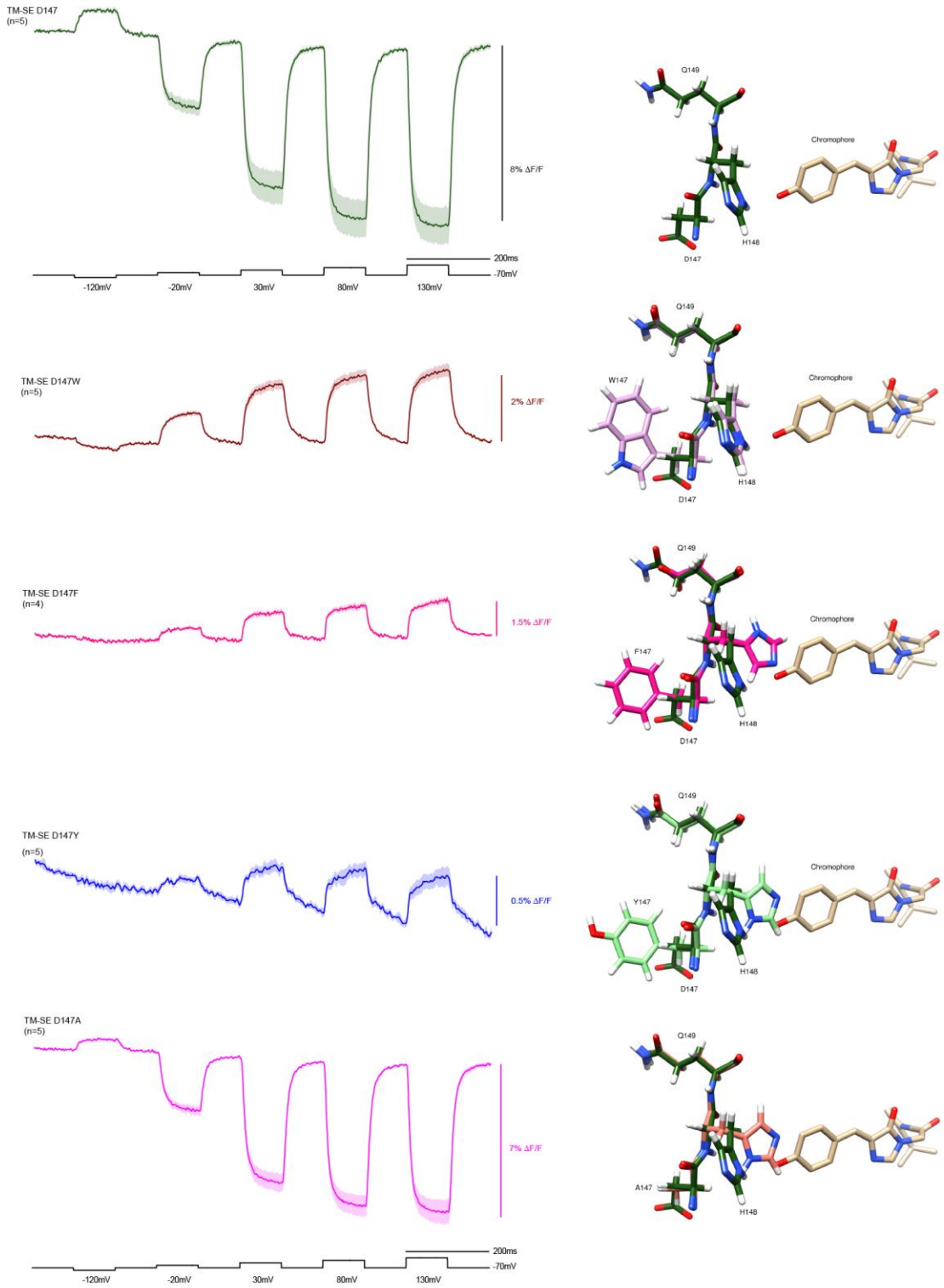
TM-SE D147
(n=5)
8% ΔF/F
200ms
-70mV
-120mV
-20mV
30mV
80mV
130mV
Q149
Chromophore
H148
D147
TM-SE D147W
(n=5)
2% ΔF/F
W147
TM-SE D147F
(n=4)
1.5% ΔF/F
F147
TM-SE D147Y
(n=5)
0.5% ΔF/F
Y147
TM-SE D147A
(n=5)
7% ΔF/F
A147

Figure 2. TM-D147X mutants affect the voltage-dependent optical signal. A. Traces on the left are the average of at least 3 HEK 293 cells under whole cell voltage clamp expressing the designated mutant version of the TM GEVI. The voltage clamp protocol is in black. The holding potential is -70 mV. The dark line in the trace is the mean and the shaded area is the standard error of the mean. On the right is the Alphafold [10] prediction of the FP domain limited to the 147, 148, and 149 residues for presentation purposes. The top structure is of the original D147 version of the FP in TM. The chromophore is from an overlaid crystal structure as explained in figure 1A. The structures below are overlays of the mutated D147X FP structure prediction from Alphafold overplayed to the original shown at top. Note the variable positioning of H148 while Q149 remains static. The framerate of fluorescence acquisition was 1 kHz. The traces were offline filtered with a 100 Hz Gaussian filter. **Figure 2. B. Aromatic residues at the D147 position invert the voltage-dependent optical signal.** Description is as in Figure 2A. The top trace is the original TM-D147 GEVI for comparison purposes.

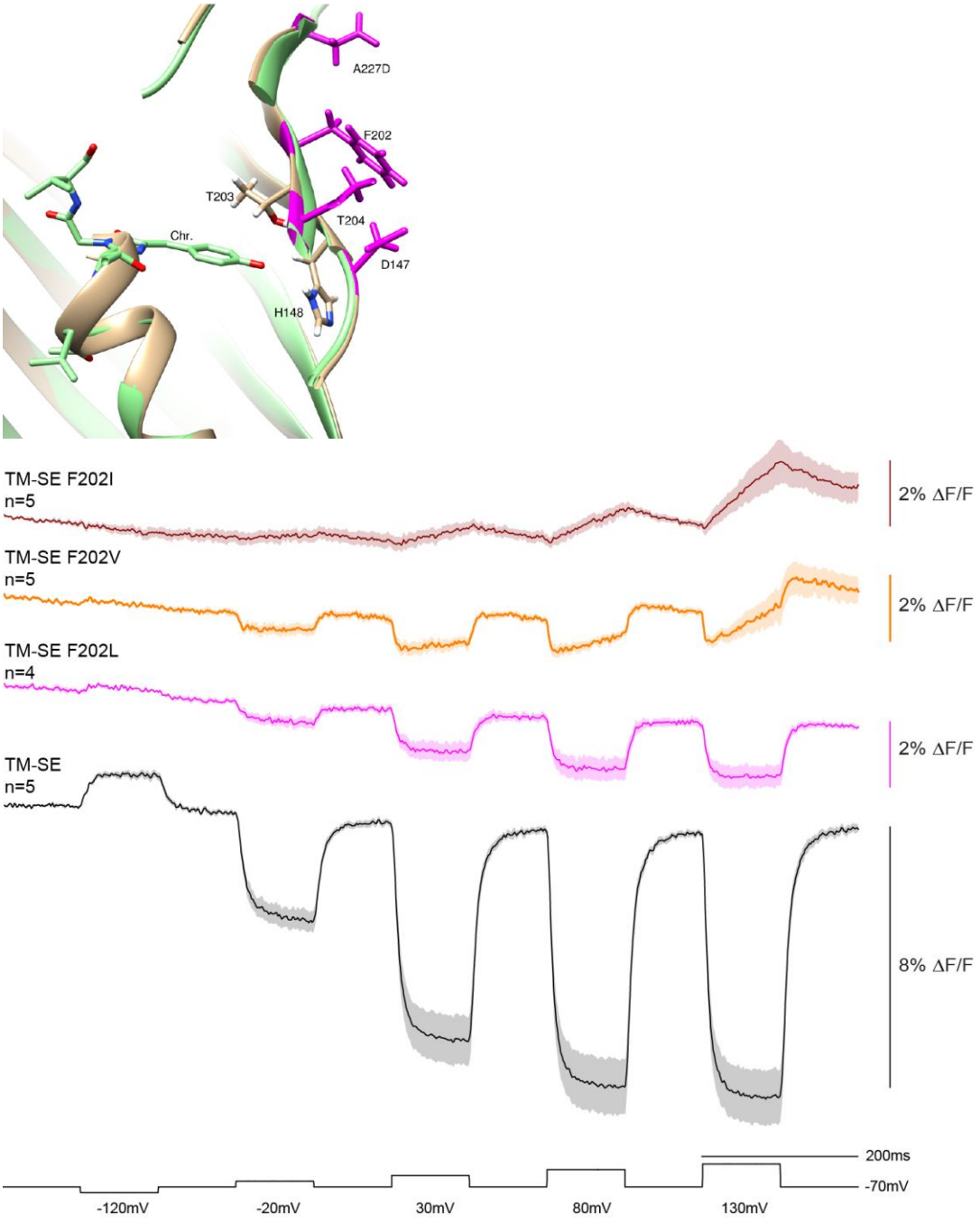

Figure 3. Side chain hydrophobicity of residue 202 in TM-SE affects the voltage-dependent fluorescence signal. The structure diagram is the insert from figure 1A showing the relative position of F202 in relation to the other external amino acids required for the large voltage-dependent optical signal [13]. The traces are from voltage clamp recordings of HEK cells expressing the respective

constructs. The command voltage is shown in black at the bottom of the figure. The dark line is the mean of at least four trials and the shaded area is the standard error of mean.

Side chain charge and orientation at position 204 in SEpH affect the voltage-dependent optical signal.

The apparent requirement for hydrophobicity at position 202 has interesting implications. There are a large number of potential hydrogen bonds along the surface of the β-barrel of GFP providing multiple avenues of potential charge displacement [2, 16]. The phenylalanine at position 202 could disrupt the hydrogen bonding network. Another possibility is that F202 is shielding and/or isolating the polar side chain at T204 which is also required for the large voltage-dependent optical signal (Figure 1A). In addition, uneven charge distribution externally flanking the internal T203 residue in the β-sheet of the barrel structure may create an inducible dipole that could alter the electrostatic environment near the chromophore upon a voltage-induced protein conformation change.

Mutations to the T204 position revealed that side chain charge as well as orientation affected the polarity of the voltage-dependent optical signal (Figure 4). When a negative charge was introduced at the 204 position, the fluorescence increased slightly for the T204D mutation while a much stronger increase in the voltage-dependent optical signal was seen for the T204E mutant. Like the 147 position, the orientation of the side chain seemed to also affect the pattern of the optical signal. Asn and Gln again differed when introduced into the 204 position. The T204R and T204H yielded only a 2% maximal dimming of the fluorescence upon a 200 mV depolarization of the plasma membrane with a multicomponent response, a fast decrease in fluorescence followed by a slower increase in fluorescence. A similar voltage-induced optical pattern could be seen in the T204Q mutant indicating that the longer side chain of Gln had positioned the nitrogen moiety of the carboxyamide group in a similar manner as to the T204R and T204H mutants. Unlike the T204Q substitution, the T204N mutant resembled the T204A mutant as well as the original T204 construct and the T204Y mutant. Interestingly, T204Y showed an improvement in the maximal signal with the fluorescence dimming about 10% for a 200 mV depolarization while the T204S construct improved the maximal decrease in fluorescence to 13.5% compared to the 8% signal seen for the original T204 version of the GEVI.

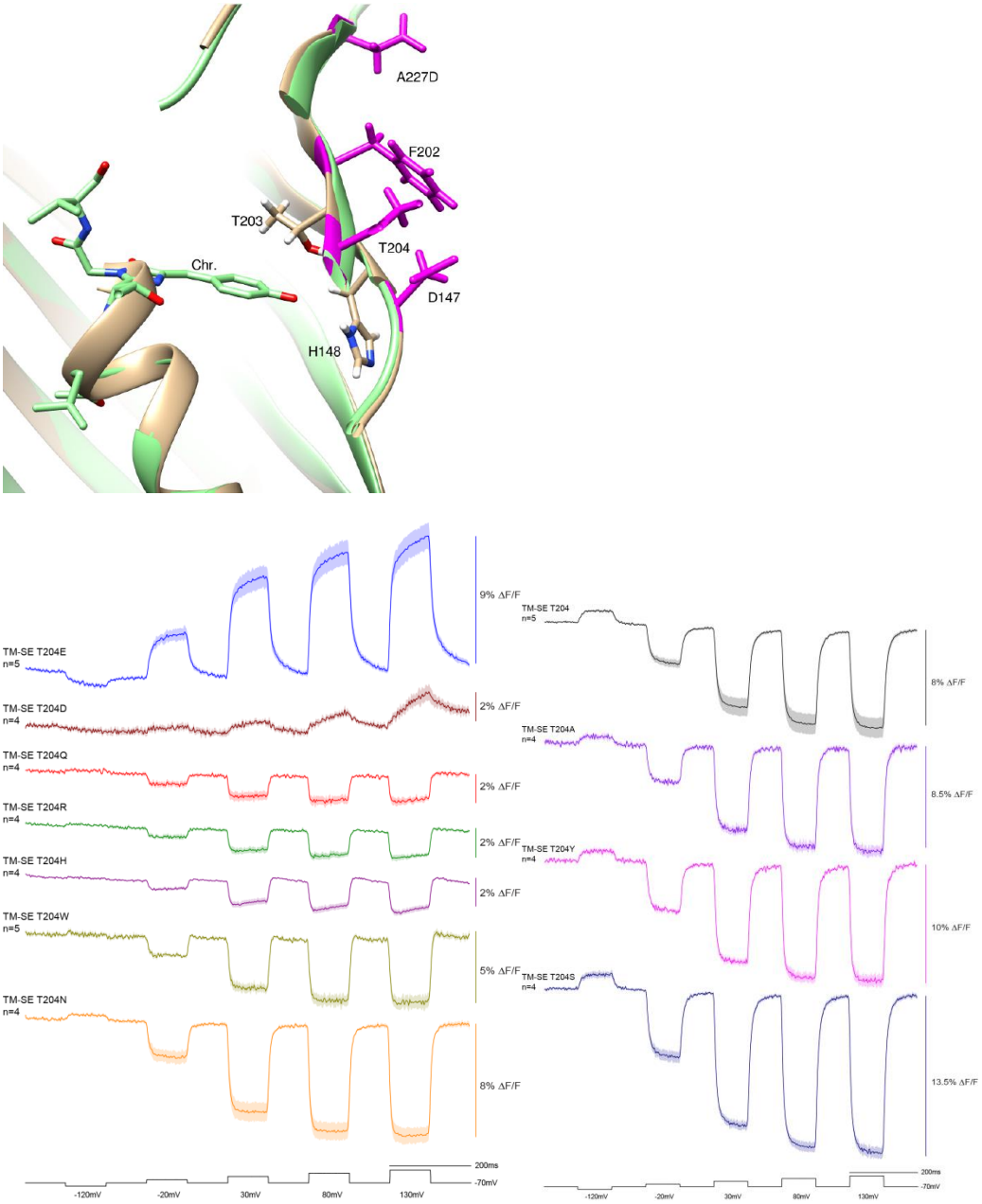

Figure 4. Charge and orientation at the 204 position of SEpH affect the voltage-dependent optical signal. The structure diagram is the insert from figure 1. T204 mutants were expressed in HEK 293 cells and subjected to whole cell voltage clamp. Solid line is the mean of at least four trials. Shaded area is the standard error of the mean.

Mutations to the internal 203 position of SEpH affect the kinetics of the voltage-dependent optical signal.

One potential conduit allowing external charge transients to affect the chromophore is the 203 position in SEpH. The hydrophobicity of the external side chain at 202 and the charge of the external side chain at position 204 affect the voltage-dependent optical signal. The internal side chain of 203 residing between those two positions is near the chromophore and has been shown to affect the fluorescence of the protein (Figure 1) [17]. Initially, we were averse to mutating internal side chain residues since it would be likely that the resting fluorescent properties of the protein would be altered in addition to the voltage-dependent signal. However, with the T204E mutant inverting the voltage-dependent optical signal, we could compare mutations at the 203 position alone and in combination with the T204E mutation to better resolve the effect on the voltage-dependent signal from that of the resting fluorescent properties (Figure 5).

In the presence of the T204E mutation, we were able to observe fluorescence in the T203E/T204E, T203Q/T204E, T203N/T204E, and the T203H/T204E double mutants (Figure 5A). T203D/T204E, T203R/T204E, and the T203K/T204E double mutants did not fluoresce. The T203E/T204E and the T203Q/T204E behave very much like the T204E single mutation in that they all exhibit an increase in fluorescence upon depolarization of the plasma membrane (compare Figures 4 and 5A). The T203N/T204E also gets brighter during depolarization steps but at a reduced level. Interestingly, the T203H/T204E double mutant gets dimmer upon depolarization of the plasma membrane. Since the T204E version gets brighter upon depolarization of the plasma membrane, the opposite effect for the T203H/T204E construct suggests that the 203 position is involved in the electrodynamic pathway from the external side chain at 204 to the internal chromophore contributing to the voltage-dependent optical signal.

In the absence of the T204E mutation, all of the T203X single mutations (in the presence of the original external side chain of T204) got dimmer in response to depolarization of the plasma membrane. There were three exceptions. The T203D, T203E, and the T203R did not fluoresce. The lack of fluorescence for T203E is noteworthy since the T203E/T204E mutant did fluoresce. In addition, the T203K single mutant fluoresced while the T203K/T204E did not. The most striking observation, however, was that a single mutation to an internal side chain in the fluorescent protein domain affected the speed of the voltage-dependent optical response of the GEVI (Figure 5B). Again, orientation of the side chain seemed to matter as the T203N slowed the optical response much like the T203K mutant while T203Q behaved like the original T203 version with a significantly faster optical response. The frame rate of acquisition was one kilohertz which is far too slow to detect differences in charge displacement implicating a corresponding rotation of the chromophore as the ultimate cause of the voltage-dependent optical signal.

A.

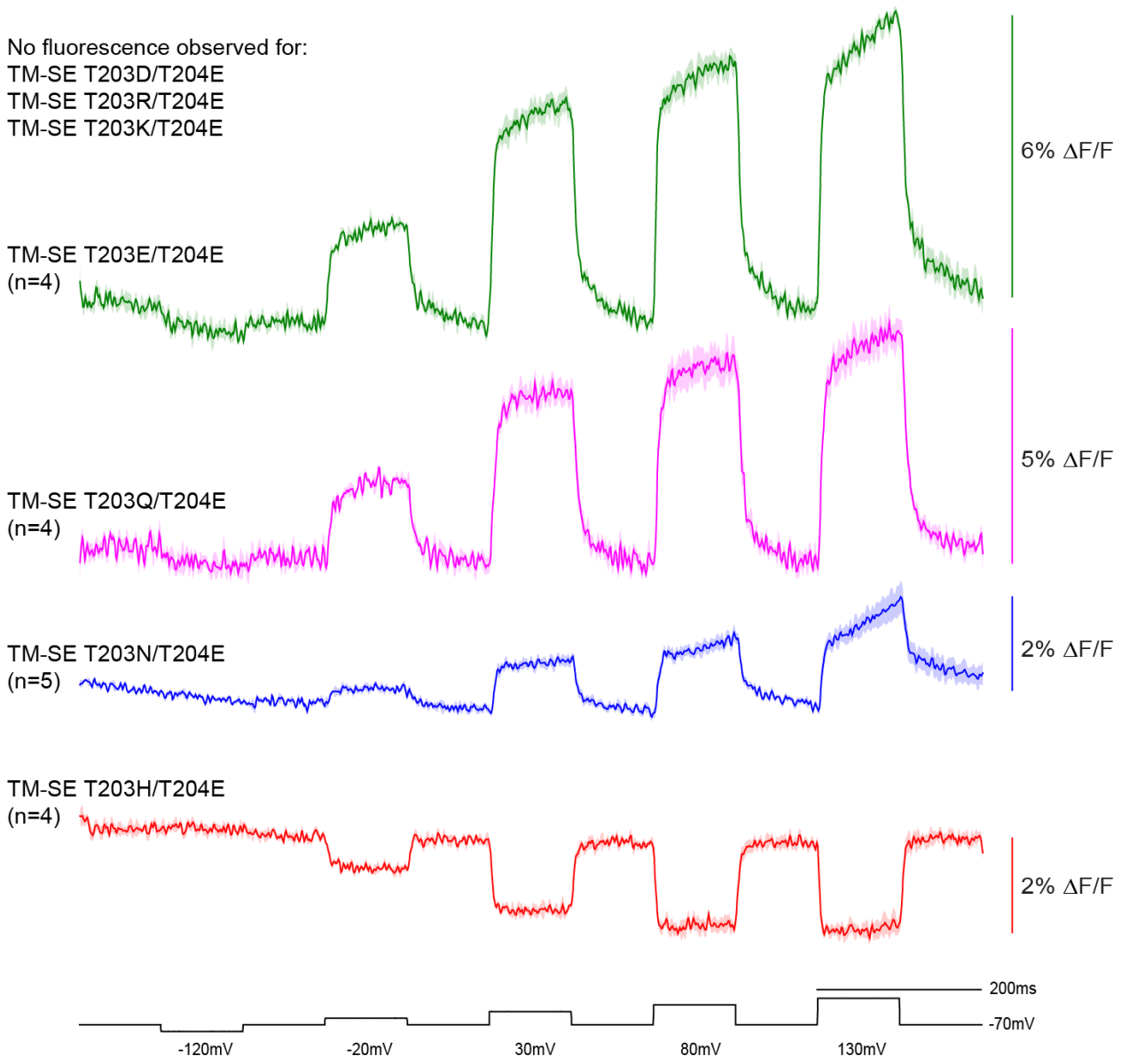
No fluorescence observed for:
TM-SE T203D/T204E
TM-SE T203R/T204E
TM-SE T203K/T204E
TM-SE T203E/T204E
(n=4)
6% ΔF/F
TM-SE T203Q/T204E
(n=4)
5% ΔF/F
TM-SE T203N/T204E
(n=5)
2% ΔF/F
TM-SE T203H/T204E
(n=4)
2% ΔF/F
200ms
-70mV
-120mV
-20mV
30mV
80mV
130mV

B.

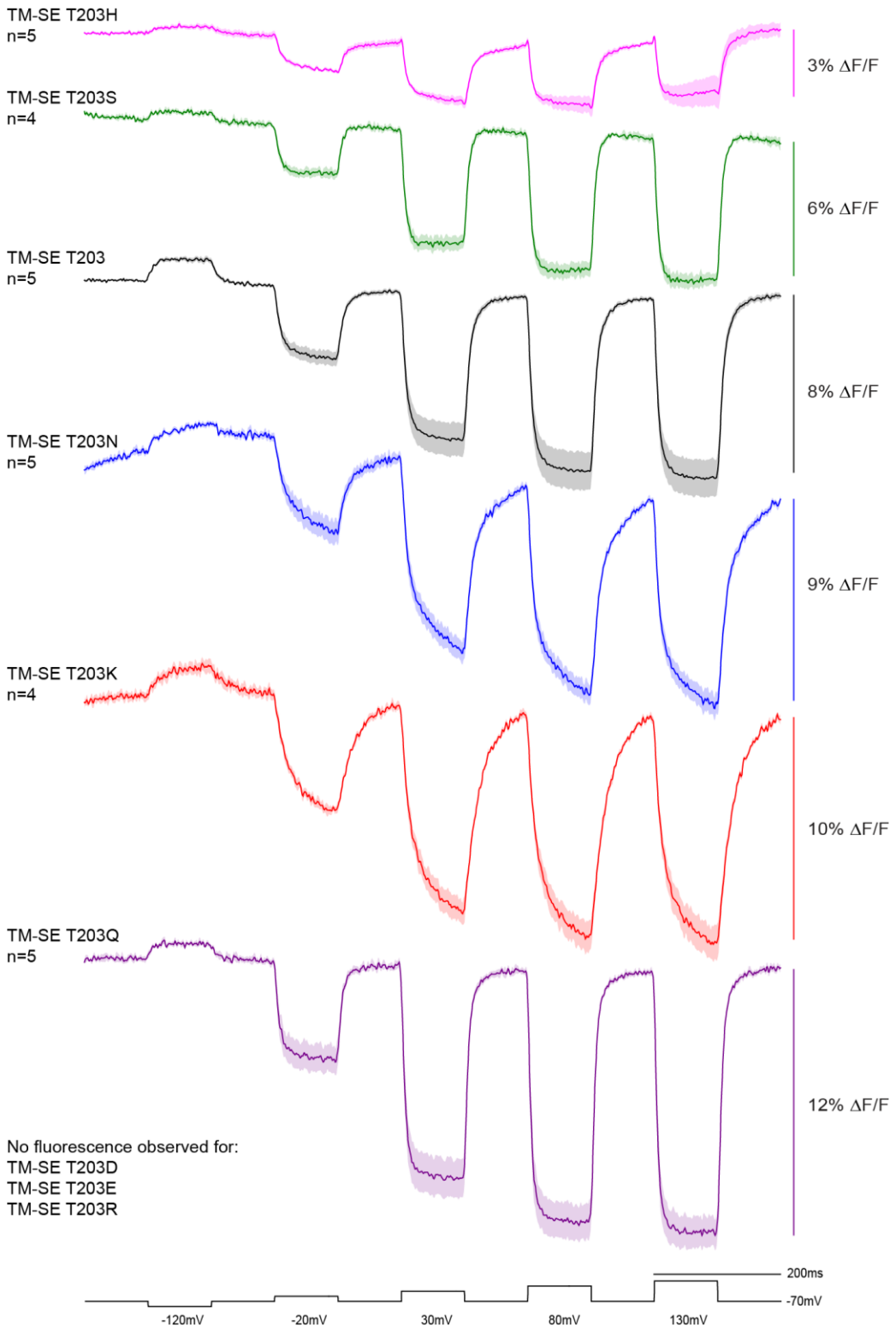
TM-SE T203H
n=5
3% ΔF/F
TM-SE T203S
n=4
6% ΔF/F
TM-SE T203
n=5
8% ΔF/F
TM-SE T203N
n=5
9% ΔF/F
TM-SE T203K
n=4
10% ΔF/F
TM-SE T203Q
n=5
12% ΔF/F
No fluorescence observed for:
TM-SE T203D
TM-SE T203E
TM-SE T203R
200ms
-70mV
-120mV
-20mV
30mV
80mV
130mV

Figure 5A. Double mutations to the T203 and T204 positions. HEK cells expressing the indicated construct were subjected to whole-cell voltage clamp and imaged at 1Khz. **Figure 5B. Mutations at the internal T203 site affect the speed of the voltage-dependent optical signal.**

The amino acid composition and length of the linker connecting the FP to the voltage sensing domain affect the path the external charge of A227D travels during voltage transients at the plasma membrane.

The increase in fluorescence for the T204E mutant could be advantageous for imaging a population of cells. Given the architecture of neurons and the distribution of their processes, a fluorescent sensor restricted to the plasma membrane that gets brighter upon neuronal activation might be easier to detect *in vivo* than a sensor that dims in response to neuronal activation [18-20]. In order to improve upon the increase in fluorescence, we introduced the T204E mutation into other GEVIs that use the FP, SEpH A227D, including ArcLight [5], Bongwoori [14], and Bongwoori-R3 [15].

The VSD and linker regions of ArcLight-derived GEVIs have been shown to affect the voltage-dependent optical signal [14, 15, 21-24]. For TM SEpH-T204E, when the VSD responds to depolarization of the plasma membrane, the fluorescence increases (Figure 4). For ArcLight with SEpH-T204E, the response is different. For a 50 mV depolarization there is an initial increase in fluorescence followed by a relatively slow decrease in fluorescence (Figure 6). When the depolarization step is increased to 100 mV, the initial increase in fluorescence is still seen but is eventually overridden by a slower decrease in fluorescence. The pattern is repeated for the 150 mV depolarization step and the 200 mV depolarization step with the initial fluorescence increase becoming a smaller component of the overall signal. For Bongwoori T204E which has a shorter linker than the ArcLight used in this study, the fluorescence only dims upon depolarization of the plasma membrane. However, for Bongwoori-R3 there is a slow increase of the voltage-dependent optical signal after an initial decrease that is not seen in Bongwoori-SE204E.

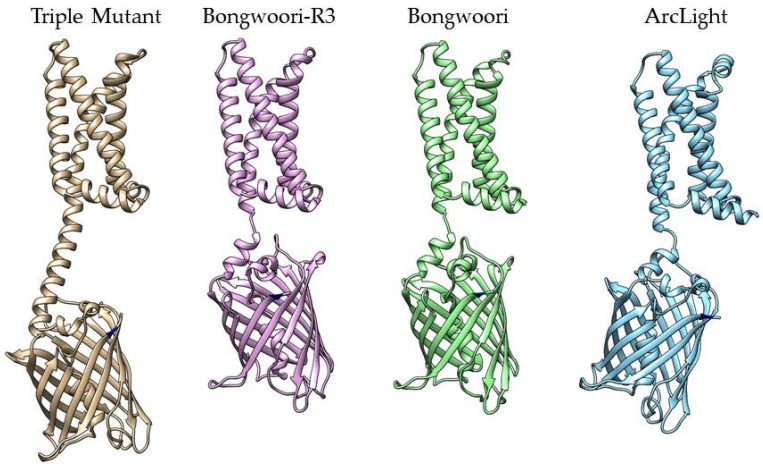
Triple Mutant
Bongwoori-R3
Bongwoori
ArcLight

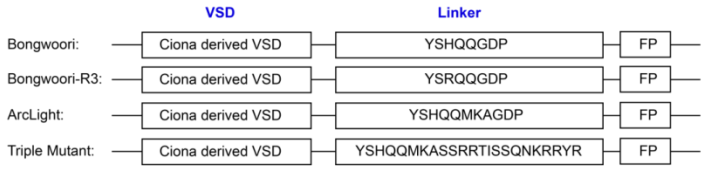
VSD
Linker
Bongwoori:
Ciona derived VSD
YSHQQGDP
FP
Bongwoori-R3:
Ciona derived VSD
YSRQQGDP
FP
ArcLight:
Ciona derived VSD
YSHQQMKAGDP
FP
Triple Mutant:
Ciona derived VSD
YSHQQMKASSRRTISSQNKRRYR
FP

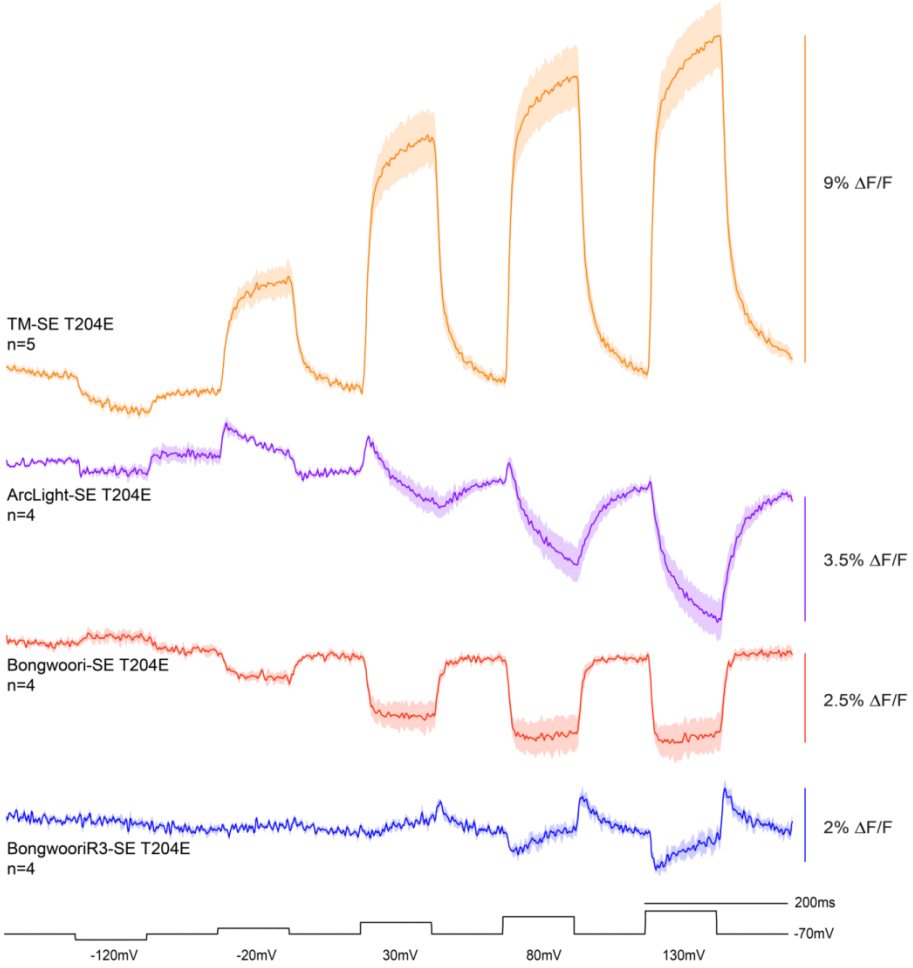
TM-SE T204E
n=5
9% ΔF/F
ArcLight-SE T204E
n=4
3.5% ΔF/F
Bongwoori-SE T204E
n=4
2.5% ΔF/F
BongwooriR3-SE T204E
n=4
2% ΔF/F
200ms
-70mV
-120mV
-20mV
30mV
80mV
130mV

Figure 6. Top structures are the Alphafold predictions of the GEVIs TripleMutant, Bongwoori-R3, Bongwoori, and Arclight. The VSD was used to align the structures to illustrate the different orientation of the FP due to linker length and composition. The schematic shows the architecture of the GEVIs with the entire amino acid sequence of the linker denoted. The TM-SE T204E trace is from figure 4 shown here for comparison purposes.

Repositioning the external negative charge yields a novel GEVI, Ulla (올라) capable of monitoring neuronal activity *in vivo*.

One potential role for the A227D mutation is an intermolecular interaction probably involving the D147 and T204 positions of a neighboring FP domain. Given the α-helical nature of the linker, the movement of S4 in the VSD upon changes in membrane potential would alter the intermolecular interactions causing the change in fluorescence. If true, this would explain the differing behaviors of the GEVIs with different linker compositions. The positioning of the FPs in relation to one another at the holding potential would be different as would be the interactions during the response of the VSD to membrane potential transients. The variation in the voltage-dependent optical signal for GEVIs of different linkers for the T204E version of the FP domain suggested that the interaction between neighboring FP domains is indeed different. The A227D mutation in SEpH may therefore not be the optimized position for the T204E version of the FP. In a previous study, the repositioning of the negative charge along the exterior of the β-barrel inverted the polarity of the voltage-dependent signal [7], so that process was repeated in the presence of the T204E mutation (Figure 7). Repositioning the negative charge along the external sites of the 11th β-strand did not invert the polarity of the optical signal; however the dynamic range was improved. The TM-T204E/L221D construct nearly doubles the dynamic range of the voltage-dependent optical signal as compared to the TM-T204E/A227D version. The best voltage-dependent optical signal was the T204E/F223D yielding a fluorescence increase greater than 25% upon a 100 mV depolarization of the plasma membrane. This new GEVI was named Ulla (올라- Korean for to ascend).

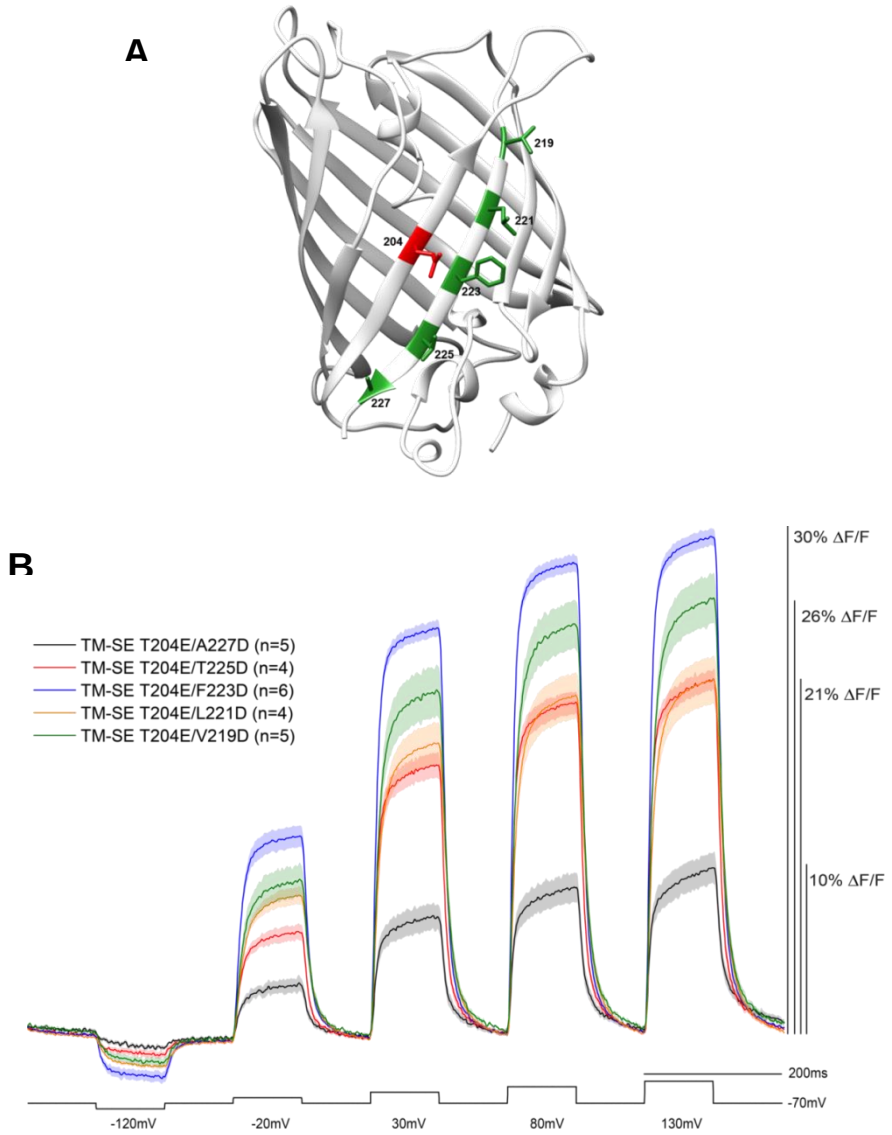

Figure 7. Repositioning the negative charge to the 223 position improves the TM-SE T204E signal. A) Position of the T204E residue and the positions of the external negative charge along the 11th beta-strand on the crystal structure of GFP from Ormö et al., 1996 (PDB: 1EMA). Annotation of the structure was done using the Chimera program (Pettersen et al., 2004). B) Optical recordings from HEK cells expressing the TM-SE T204E construct with the external negative charge at the A227D position (black trace), T225D position (red trace), F223D position (blue trace), L221D position (orange trace), and V219D position (green trace). The command voltage is shown in black at the bottom of the figure. The dark lines represent the mean and the shaded areas represent that standard error of the mean.

Population signals from the novel GEVI, Ulla.

A GEVI that gets 25% brighter upon depolarization of the plasma membrane offers an exciting new tool for discerning the activity of neuronal circuits. Voltage imaging poses many challenges, not the least of which is having a functional probe that is restricted to the plasma membrane [25]. With the fluorescence distributed along the surface of neurons, the interspersion of neuronal processes

generates a relatively high background fluorescence that can make it difficult to observe action potentials let alone synaptic inputs. Having a GEVI that gets brighter enables the flexibility of illumination intensities to further reduce the resting fluorescence.

Imaging mouse hippocampal CA1 in brain slice at 5 kHz using variable light levels.

Imaging neuronal activity in the CA1 region of the hippocampus was achieved by injection of an AAV coding for Ulla under the control of the hSynapsin promoter (Figure 8A). Two weeks after injection, optical measurements from hippocampal brain slices during Schaffer collateral electrical stimulation were recorded (Figure 8B). Upon Schaffer collateral stimulation a rapid increase in fluorescence could be detected near the stimulating electrode corresponding to neurons experiencing a depolarization of the plasma membrane (Figure 8C). The deplorization is quickly followed by a decrease in fluorescence corresponding to neuronal inhibition previously observed in the CA1 region of the hippocampus with the GEVI ArcLight [26, 27]. While the excitatory signal is not large (0.2% $\Delta F/F$), the event is easily observed in a single trial due to a robust Signal-to-Noise Ratio (SNR) of 22.

The ability of Ulla to get brighter when a neuron is activated enables the use of low light levels. To illustrate this point, we imaged the CA1 region in brain slice again during electrical stimulation of the Schaffer collaterals at different excitation light levels (Figure 8D). We also increased the imaging frame rate to 5 kHz to further reduce the amount of light detected per frame. The results are rather impressive. At the lowest setting of the LED (500 mW/cm^2), a signal again of 0.2% $\Delta F/F$ could be seen though the SNR is poor (<2). The signal size remained consistent over multiple trials resulting in an improvement of the SNR. Alternatively, a high SNR could also be achieved in a single trial during 5 kHz acquisition by increasing the excitation light to 13 W/cm^2. Light levels can therefore be adjusted to reduce the background fluorescence of the circuit being investigated.

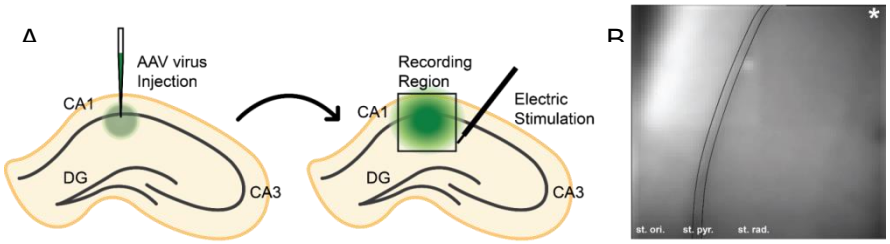
A
AAV virus
Injection
CA1
DG
CA3
Recording
Region
Electric
Stimulation
CA1
DG
CA3
B
st. ori.
st. pyr.
st. rad.

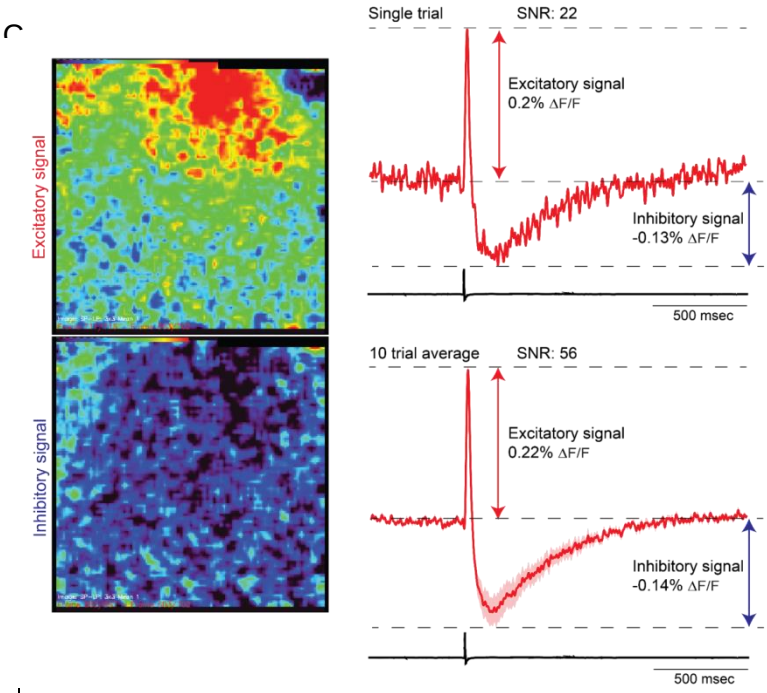
C
Excitatory signal
Inhibitory signal
Single trial
SNR: 22
Excitatory signal
0.2% ΔF/F
Inhibitory signal
-0.13% ΔF/F
500 msec
10 trial average
SNR: 56
Excitatory signal
0.22% ΔF/F
Inhibitory signal
-0.14% ΔF/F
500 msec

D.

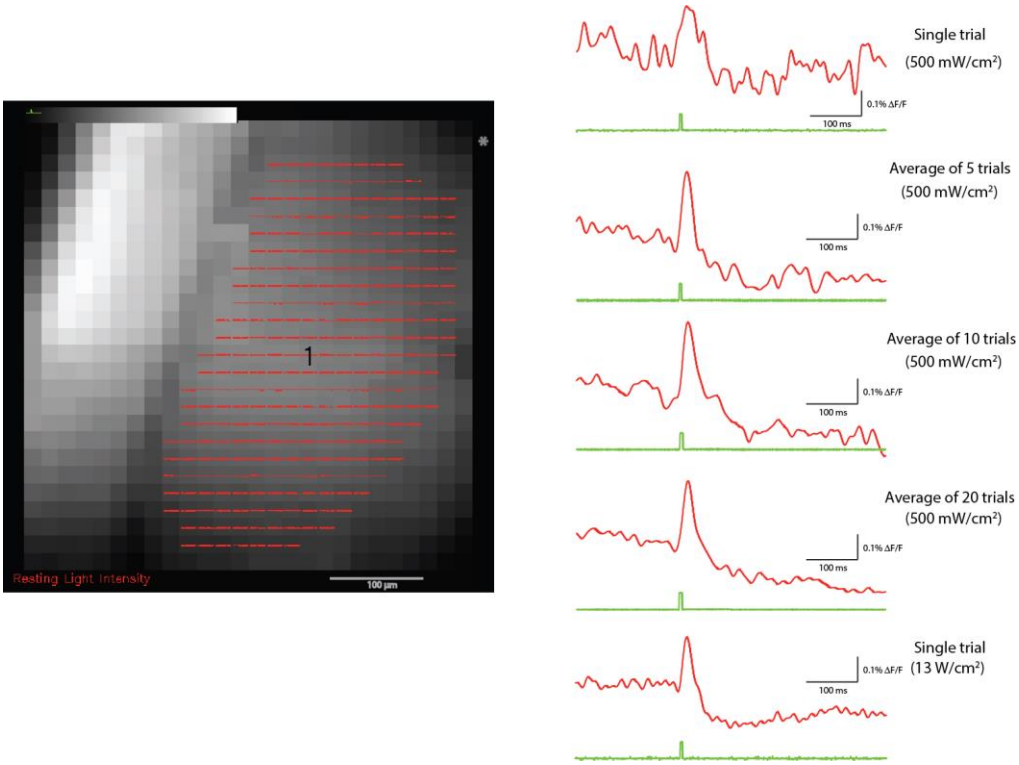
1
Resting Light Intensity
100 µm
Single trial
(500 mW/cm²)
0.1% ΔF/F
100 ms
Average of 5 trials
(500 mW/cm²)
Average of 10 trials
(500 mW/cm²)
Average of 20 trials
(500 mW/cm²)
Single trial
(13 W/cm²)

Figure 8. Population signals in mouse hippocampal acute brain slice. A. Schematic of the experimental design. B. Resting fluorescence of Ulla in the CA1 region of the hippocampus. C. Heat maps and optical traces of the fluorescence change in response to electrical stimulation of the Schaffer collaterals. Heat map of the excitation signal corresponds to the fluorescence peak shown in the optical trace. Heat map of the inhibition signal corresponds to the fluorescence minimum following the excitation peak. Frame rate acquisition was 1 kHz. D. Monitoring Ulla fluorescence during electrical stimulation of the Schaffer collaterals under varying light levels. Framerate of acquisition was 5 kHz. A stimulating electrode (*) was used to excite Schaffer collateral axons. The stimulation is shown in green and the fluorescence is shown in red.

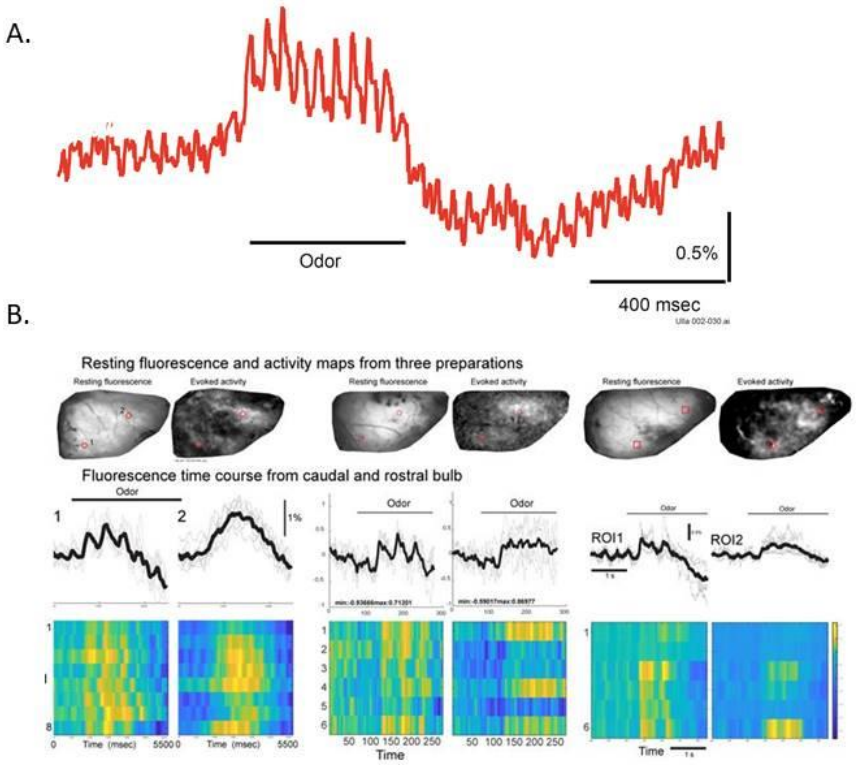

Figure 9. Population recordings of Ulla (올라) in the olfactory bulb. A. Single trial optical response from an anesthetized mouse. B. Consistency of fluorescence response across multiple trials in three mice.

In vivo imaging of Ulla from the dorsal olfactory bulb.

In each preparation an adeno-associated virus (AAV) expressing Ulla was injected into one olfactory bulb. To examine the relative brightness of Ulla in comparison to endogenous fluorescence present in the brain, we exposed both hemibulbs in each preparation, and simultaneously quantified the fluorescence emission from both hemibulbs (Figure 9). The injected side was 2.2 ± 0.5-fold brighter than the uninjected side (1.85-3.02 brighter, N = 4 preparations, p = 0.02 using a ranksum test). Thus, Ulla results in significantly brighter fluorescence emission than endogenous fluorescence emission when using this particular serotype promoter combination.

Next we examined the ability of Ulla to report odor-evoked signals in anesthetized mice (Figure 9A). The odor methyl valerate was presented between 1-6% of saturated vapor for 3 seconds. The odor evoked spatially distinct patterns of activity across the dorsal surface of the bulb in all preparations tested. In each preparation we measured the response to a region of interest located in the caudal and rostral bulb (Figure 9B). Figure 9B illustrates the mean response from the ROIs in each preparation where the trials were aligned to the onset of the response (Figure 9B; thick black lines). Moreover, the two regions

had distinct response dynamics, where the caudal region of interest exhibited distinct oscillations consistent with the animal's respiratory pattern; while the rostral glomerulus tended to be slower and more sustained (Figure 9B, compare 1 vs 2). Overall, the SNR and response dynamics were relatively stable across the single trials and comparable to those seen with ArcLight [28] (Figure 9B, bottom heat maps). The average response across all regions of interest in 3 preparations was 0.76 ± 0.28 ΔF/F (the response from the caudal and rostral ROI was measured in 4-5 trials for each preparation and averaged together; range: 0.38-1.07 ΔF/F). Thus, we conclude that Ulla is a GEVI with sufficient brightness and SNR to detect odor-evoked signals *in vivo*.

Conclusion

The serendipitous mutation placing a novel negative charge on the surface of the FP domain of the GEVI, ArcLight, has not only allowed the optical monitoring of neuronal circuits [29] [28] but also offers a new way to visualize charge migration through a fluorescent protein. The voltage-induced conformational change of ArcLight-derived GEVIs induces an electrodynamic response in the FP domain. These electrodynamic responses alter the optical properties of the chromophore and involve amino acids with side chains oriented on both the outer and inner surfaces of the β-barrel.

Voltage transients at the plasma membrane cause the VSD to change conformation [30-33]. Comparison of the crystal structures of the VSD from *Ciona* voltage-dependent phosphatase in the up and down states reveals a 5 Å displacement as well as a 60° rotation of the S4 transmembrane segment [11]. Based on the Alphafold prediction of the ArcLight structure (Figure 1), the FP linked to the VSD would also move. Yet movement of the FP alone cannot explain the change in fluorescence.

Previous reports have shown that the FP domains of neighboring ArcLight-type GEVIs interact. For example, an intermolecular-FRET signal is seen when SEpH is replaced with either a FRET donor or a FRET acceptor FP domain (Figure 1) [9]. The electrostatic environment surrounding the chromophore is also altered when conformational change of the protein occurs as the proton wire enabling the long Stokes shift of SEpH can be enhanced in a voltage-dependent manner [7]. These observations suggest that the negative charge (A227D) on the FP domain of ArcLight can alter the optical properties by interacting with a neighboring FP domain.

To explore potential pathways of charge migration through the FP domain of ArcLight-type GEVIs, mutations to the surface as well as to the interior of the FP domain were performed while keeping the VSD and linker domain of the GEVI constant. At multiple positions in the FP domain, the orientation of the side chain affected the voltage-dependent optical signal mutations. For instance, mutations at position 147 of the FP domain yielded three distinct optical responses upon depolarization of the plasma membrane (Figures 2A and 2B). The D147K mutant had a much reduced signal during both depolarization and hyperpolarization of the plasma membrane while the D147T was very much like the original D147 version. Despite Asn and Gln having the same carboxyamide functional group in their side chains, the D147Q mutant exhibited an optical response similar to the amino acids with hydroxyl or

carboxyl groups in their side chains while the D147N construct behaved in a very similar manner to the D147K mutant (Figure 2A).

The lack of structural data hinders our understanding of how the role of hydrogen bonds affects the differing voltage-dependent optical signals of the D147N and D147Q mutants (Figure 2). The original D147 version of the GEVI, TM, yields a characteristic voltage-dependent optical signal that the D147T, D147S, and the D147Q mutations also exhibit. Introducing a positively charged amino acid at this position (D147K) significantly reduces the voltage-dependent optical signal and introduces multiple components with an initial decrease followed by a slow increase in fluorescence. However, the positive charge at position 147 does not seem to play a role as the polar D147N mutant exhibits a remarkably similar pattern. Amino acids therefore with nitrogen present in their sidechains behave one way, while the oxygen of the hydroxyl and carboxyl groups in Ser, Thr, and Asp behave in another. Yet, the same carboxyamide found in the sidechains of Asn and Gln differ in the voltage-dependent optical signal suggesting that the orientation of the nitrogen and oxygen of those sidechains determines the type of signal seen.

Hydrophobic amino acids play an important role in charge migration through the FP. The introduction of amino acids with aromatic side chains at the 147 position resulted in a third distinct voltage-dependent optical signal that exhibited an increase in the fluorescence upon depolarization of the plasma membrane (Figure 2B). The presence of a large aromatic ring may inhibit charge interactions at this position allowing alternate pathways to influence the fluorescence of the GEVI. The 202 and 204 positions have also been implicated in the large voltage-dependent optical signal of ArcLight [5]. These two positions with their side chains oriented towards the exterior of the β-barrel flank the 203 position that has an internally oriented side chain positioned near the chromophore. During the generation of the pH-sensitive SEpH, the 202 position was converted from a Ser to Phe. When this mutation was reverted back to Ser from Phe, the voltage-dependent signal was significantly diminished [13]. Conservative substitutions at position 202 reducing the side chain surface area of Phe to Leu or Val diminished the voltage-dependent optical signal by over 4-fold (Figure 3). The F202I mutation again inverts the signal yielding a very slow and small fluorescence increase upon depolarization of the plasma membrane.

Mutations to the 204 position also revealed a side chain orientation dependent optical response upon depolarization of the plasma membrane (Figure 4). Once again, Gln and Asn exhibited different responses when introduced to the 204 position. However, unlike the 147 position, the T204Q behaved in a similar manner to T204R and T204H while T204N exhibited a voltage-dependent optical signal similar to T204S as well as the original T204 construct. Another difference at the 204 position was the effect of a negative charge. The T204D caused a small increase in the fluorescence upon depolarization of the plasma membrane. The T204E was even better yielding a near 10% increase in fluorescence of 100 mV depolarization step.

Double mutation of the FP domain at positions 203 and 204 revealed that the voltage-dependent optical signal operates at least in part through the 204-203 pathway (Figure 5A). The T203E/T204E mutant

increased fluorescence upon depolarization of the plasma membrane as did the T203Q/T204E and T203N/T204E constructs. However, the T203H/T204E got dimmer when the plasma membrane was depolarized indicating that the 203 position can reverse the polarity of the optical signal exhibited by the T204E single mutation.

All of the 203 mutants that fluoresced exhibited a decrease in the fluorescence upon depolarization of the plasma membrane (Figure 5B). Remarkably, the T203K and T203N mutants slowed the voltage-dependent optical signal. An internal residue in the FP domain slowing the optical response is a strong indicator that the electrostatic environment inside the β-barrel is altered upon a voltage-induced conformational change resulting in the rotation of internal chemical groups. This leads to the model that the chemistry on the surface of the β-barrel contributes to the orientation of the chromophore via internal side chains in close proximity to the chromophore. The voltage-dependent optical signal results from a twist in the chromophore that either reduces the planarity (dims the fluorescence) or improves the planarity (increases the fluorescence) [34].

This model has several requirements. First there exists an electrostatic potential across the chromophore that affects its planarity. Molecular simulations involving the chromophore of several FPs suggests that the electrostatic potential inside the β-barrel plays a larger role than steric effects in maintaining the rigidity of the chromophore [35]. In the case of SEpH, the H148 and T203 side chains are in close proximity to chromophore and may well contribute to the electrostatic potential determining the planarity of the chromophore. Electrical manipulation of H148 and/or T203 could then alter the internal potential resulting in a twist of the chromophore.

The second requirement is that the internal electrical environment must be dynamic; it must be able to respond to environmental conditions. The pH dependence of SEpH and the voltage-dependent enhancement of the fluorescence upon excitation at 390 nm for the GEVI TM-SEpHT65/H222 suggests that the internal electrical environment of the FP domain is indeed dynamic [7] allowing multiple configurations to restore the proton wire required for the large Stoke shift.

How do ArcLight-derived GEVIs alter the internal potential of the FP domain? The structure of the β-sheet places the side chains of the amino acids flanking H148 and T203 on the exterior of the protein. Asymmetric charge distribution at positions F202 and T204 may create an inducible dipole for T203 resulting in a pathway for external interactions to affect the fluorescence of the protein. For H148, an added confound is the potential conformational flexibility as demonstrated by the Alphafold predictions (Figures 2 and 3). While these predictions may be incorrect, this potential flexibility of H148 may explain the behavior of the D147 mutants. Indeed, the distinct behavior of Asn mutants compared to Gln substitutions suggests that hydrogen bonds may also contribute to the electrical properties of the external surface ultimately affecting the voltage-dependent optical signal. Of course, structural data and modeling will be required to better address these issues, but ArcLight-derived GEVIs offer novel functional observations to test these models.

A third requirement would be a consistent means of inducing a change in the internal electrostatic potential. This is likely the role of the A227D that is also required for the large voltage-dependent optical signal of ArcLight. This negative charge would interact with the potential 'hotspots' at D147 and T204 of a neighboring FP domain. Voltage transients at the plasma membrane would then cause a conformational change that would alter that interaction resulting in a twist of the chromophore. Lending support to this role is the divergent behavior of the T204E mutants in ArcLight versus TM, Bongwoori or Bongwoori-R3 (Figure 6) and the optimization of the signal via the Asp scan (Figure 7). Different linker lengths between the VSD and the FP domain would alter the starting position of A227D in relationship to the neighboring FP domain as well as affect the path travelled during the voltage-induced conformational change.

Our exploration of the mechanism responsible for the voltage-dependent optical signal has yielded a novel GEVI that yields an SNR comparable to ArcLight *in vivo* with the added benefit of a GEVI that gets brighter in response to depolarization of the plasma membrane (Figures 8 and 9). The ability to optically report neuronal activities at a 5 kHz acquisition rate in low light levels offers the experimenter more control over the recording conditions during the experiment. For instance, the excitation light intensity can be adjusted to diminish the background fluorescence thereby enhancing the detection of depolarizing events during the recording. Ulla therefore provides a new tool for imaging voltage in neuronal circuits as well as for investigating the photophysics of fluorescent proteins.

Acknowledgements

We thank Lawrence B. Cohen for critical review of the manuscript. We thank J. E. Dotzlaf and A. J. Kreuzman for insights into protein structure and function. Molecular graphics and analyses performed with UCSF Chimera, developed by the Resource for Biocomputing, Visualization, and Informatics at the University of California, San Francisco, with support from NIH P41-GM103311. This study was funded by Korea Institute of Science and Technology grant 2E31523.

References

1. Chattoraj, M., et al., *Ultra-fast excited state dynamics in green fluorescent protein: multiple states and proton transfer.* Proc Natl Acad Sci U S A, 1996. **93**(16): p. 8362-7.
2. Shinobu, A. and N. Agmon, *Proton Wire Dynamics in the Green Fluorescent Protein.* J Chem Theory Comput, 2017. **13**(1): p. 353-369.
3. Di Donato, M., et al., *Proton transfer events in GFP.* Phys Chem Chem Phys, 2011. **13**(36): p. 16295-305.
4. Lossau, H., et al., *Time-resolved spectroscopy of wild-type and mutant Green Fluorescent Proteins reveals excited state deprotonation consistent with fluorophore-protein interactions.* Chemical Physics, 1996. **213**(1): p. 1-16.
5. Jin, L., et al., *Single action potentials and subthreshold electrical events imaged in neurons with a fluorescent protein voltage probe.* Neuron, 2012. **75**(5): p. 779-85.

6. Miesenbock, G., D.A. De Angelis, and J.E. Rothman, *Visualizing secretion and synaptic transmission with pH-sensitive green fluorescent proteins.* Nature, 1998. **394**(6689): p. 192-5.
7. Kang, B.E., et al., *Mechanism of ArcLight derived GEVIs involves electrostatic interactions that can affect proton wires.* Biophys J, 2021.
8. Rayaprolu, V., et al., *Dimerization of the voltage-sensing phosphatase controls its voltage-sensing and catalytic activity.* J Gen Physiol, 2018. **150**(5): p. 683-696.
9. Leong, L.M., B.E. Kang, and B.J. Baker, *Improving the flexibility of genetically encoded voltage indicators via intermolecular FRET.* Biophys J, 2021.
10. Jumper, J., et al., *Highly accurate protein structure prediction with AlphaFold.* Nature, 2021. **596**(7873): p. 583-589.
11. Li, Q., et al., *Structural mechanism of voltage-dependent gating in an isolated voltage-sensing domain.* Nat Struct Mol Biol, 2014. **21**(3): p. 244-52.
12. Arpino, J.A., P.J. Rizkallah, and D.D. Jones, *Crystal structure of enhanced green fluorescent protein to 1.35 A resolution reveals alternative conformations for Glu222.* PLoS One, 2012. **7**(10): p. e47132.
13. Han, Z., et al., *Mechanistic studies of the genetically encoded fluorescent protein voltage probe ArcLight.* PLoS One, 2014. **9**(11): p. e113873.
14. Piao, H.H., et al., *Combinatorial mutagenesis of the voltage-sensing domain enables the optical resolution of action potentials firing at 60 Hz by a genetically encoded fluorescent sensor of membrane potential.* J Neurosci, 2015. **35**(1): p. 372-85.
15. Lee, S., et al., *Improving a genetically encoded voltage indicator by modifying the cytoplasmic charge composition.* Scientific Reports, 2017. **7**(1): p. 8286.
16. Shinobu, A., et al., *Visualizing proton antenna in a high-resolution green fluorescent protein structure.* J Am Chem Soc, 2010. **132**(32): p. 11093-102.
17. Ormo, M., et al., *Crystal structure of the Aequorea victoria green fluorescent protein.* Science, 1996. **273**(5280): p. 1392-5.
18. Nakajima, R., et al., *Optogenetic Monitoring of Synaptic Activity with Genetically Encoded Voltage Indicators.* Front Synaptic Neurosci, 2016. **8**: p. 22.
19. Platisa, J., et al., *Directed Evolution of Key Residues in Fluorescent Protein Inverses the Polarity of Voltage Sensitivity in the Genetically Encoded Indicator ArcLight.* ACS Chem Neurosci, 2017. **8**(3): p. 513-523.
20. Abdelfattah, A.S., et al., *A Bright and Fast Red Fluorescent Protein Voltage Indicator That Reports Neuronal Activity in Organotypic Brain Slices.* J Neurosci, 2016. **36**(8): p. 2458-72.
21. Jung, A., et al., *Linker length and fusion site composition improve the optical signal of genetically encoded fluorescent voltage sensors.* Neurophotonics, 2015. **2**(2): p. 021012.
22. Kang, B.E. and B.J. Baker, *Pado, a fluorescent protein with proton channel activity can optically monitor membrane potential, intracellular pH, and map gap junctions.* Sci Rep, 2016. **6**: p. 23865.
23. Baker, B.J., et al., *Genetically encoded fluorescent voltage sensors using the voltage-sensing domain of Nematostella and Danio phosphatases exhibit fast kinetics.* J Neurosci Methods, 2012. **208**(2): p. 190-6.
24. Jung, A., et al., *Modulating the Voltage-sensitivity of a Genetically Encoded Voltage Indicator.* Exp Neurobiol, 2017. **26**(5): p. 241-251.
25. Rhee, J.K., et al., *Biophysical Parameters of GEVIs: Considerations for Imaging Voltage.* Biophys J, 2020.
26. Nakajima, R. and B.J. Baker, *Mapping of excitatory and inhibitory postsynaptic potentials of neuronal populations in hippocampal slices using the GEVI, ArcLight.* Journal of Physics D: Applied Physics, 2018. **51**(50).

27. Nakajima, R., et al., *GEVI cell-type specific labelling and a manifold learning approach provide evidence for lateral inhibition at the population level in the mouse hippocampal CA1 area.* Eur J Neurosci, 2021.
28. Storace, D.A. and L.B. Cohen, *Measuring the olfactory bulb input-output transformation reveals a contribution to the perception of odorant concentration invariance.* Nat Commun, 2017. **8**(1): p. 81.
29. Bando, Y., et al., *Comparative Evaluation of Genetically Encoded Voltage Indicators.* Cell Rep, 2019. **26**(3): p. 802-813 e4.
30. Yang, N. and R. Horn, *Evidence for voltage-dependent S4 movement in sodium channels.* Neuron, 1995. **15**(1): p. 213-8.
31. Yang, N., A.L. George, Jr., and R. Horn, *Molecular basis of charge movement in voltage-gated sodium channels.* Neuron, 1996. **16**(1): p. 113-22.
32. Mannuzzu, L.M., M.M. Moronne, and E.Y. Isacoff, *Direct physical measure of conformational rearrangement underlying potassium channel gating.* Science, 1996. **271**(5246): p. 213-6.
33. Cha, A. and F. Bezanilla, *Characterizing voltage-dependent conformational changes in the Shaker K+ channel with fluorescence.* Neuron, 1997. **19**(5): p. 1127-40.
34. Martin, M.E., F. Negri, and M. Olivucci, *Origin, nature, and fate of the fluorescent state of the green fluorescent protein chromophore at the CASPT2//CASSCF resolution.* J Am Chem Soc, 2004. **126**(17): p. 5452-64.
35. Park, J.W. and Y.M. Rhee, *Electric Field Keeps Chromophore Planar and Produces High Yield Fluorescence in Green Fluorescent Protein.* J Am Chem Soc, 2016. **138**(41): p. 13619-13629.

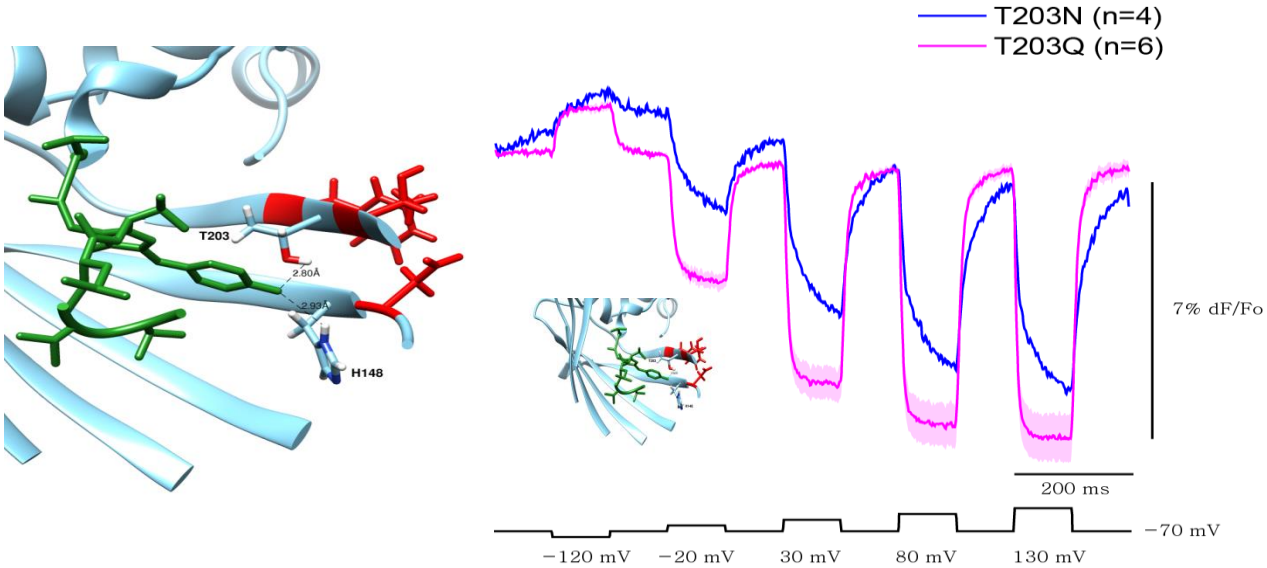
T203
2.80Å
2.93Å
H148
T203N (n=4)
T203Q (n=6)
7% dF/Fo
200 ms
−70 mV
−120 mV
−20 mV
30 mV
80 mV
130 mV